Supporting information for:

Charged Surface-Active Impurities At Nanomolar Concentration Induce Jones-Ray Effect

Yuki Uematsu,[†,‡] Douwe Jan Bonthuis,[‡] and Roland R. Netz[*,‡]

†*Department of Chemistry, Kyushu University, Fukuoka 819-0395, Japan*

‡*Fachbereich Physik, Freie Universität Berlin, 14195 Berlin, Germany*

E-mail: rnetz@physik.fu-berlin.de

Contents

S1 Analytic solution of the Poisson-Boltzmann equation

We describe the analytic solution of

$$\varepsilon\varepsilon_0 \frac{d^2\psi}{dz^2} = -e \sum_i q_i c_i^{\rm b} {\rm e}^{-q_i e\psi/k_{\rm B}T - \alpha_i\theta(z^*-z)} \quad \text{for} \quad 0 < z, \tag{S1}$$

with boundary conditions $d\psi/dz|_{z=0} = 0$ and $\psi(z \to \infty) = 0$. For the case of two ionic species $(i = +, -)$ the analytic solution is given by

$$\psi(z) = \frac{2k_{\rm B}T}{e} \ln \frac{1 + {\rm e}^{-\kappa(z-z^*)} \tanh(\Psi^*/4)}{1 - {\rm e}^{-\kappa(z-z^*)} \tanh(\Psi^*/4)} \quad \text{for} \quad z > z^*, \tag{S2}$$

and

$$\psi(z) = \frac{k_{\rm B}T}{e} \left[\ln \frac{1 + \sigma {\rm dn}(x(z)|m)}{1 - \sigma {\rm dn}(x(z)|m)} + \Delta\Psi \right] \quad \text{for} \quad 0 < z < z^*, \tag{S3}$$

where $\kappa = \sqrt{e^2(c_+^{\rm b} + c_-^{\rm b})/\varepsilon\varepsilon_0 k_{\rm B}T}$, $\Psi^* = e\psi(z^*)/k_{\rm B}T$, $\Delta\Psi = -(\alpha_+ - \alpha_-)/2$, $\sigma = {\rm sgn}(\alpha_+ - \alpha_-)$,

$$x(z) = -\frac{\kappa(z - z^*)}{{\rm e}^{(\alpha_+ + \alpha_-)/4}\sqrt{m}} + {\rm dn}^{-1}\left(\left| \frac{1 - {\rm e}^{\Psi^* - \Delta\Psi}}{1 + {\rm e}^{\Psi^* - \Delta\Psi}} \right| \right), \tag{S4}$$

$$m = \left[\cosh^2\left(\frac{\Psi^* - \Delta\Psi}{2} \right) - {\rm e}^{\frac{\alpha_+ + \alpha_-}{2}} \sinh^2\left(\frac{\Psi^*}{2} \right) \right]^{-1}, \tag{S5}$$

and ${\rm dn}(x|m)$ denotes the Jacobian elliptic function.[S1] The boundary condition $d\psi/dz|_{z=0} = 0$ leads to

$$x(0) = K(m), \tag{S6}$$

which determines Ψ^*, where $K(m)$ is the complete elliptic function of the first kind.[S1] For the case with more than two ionic species, we use the same analytic solution and define $c_i^{\rm b}$-dependent $\alpha_\pm$. For example, for four species we obtain

$$\alpha_+ = -\ln\left(\frac{c_{\rm Na}^{\rm b} {\rm e}^{-\alpha_{\rm Na}} + c_{\rm cou}^{\rm b} {\rm e}^{-\alpha_{\rm cou}}}{c_{\rm Na}^{\rm b} + c_{\rm cou}^{\rm b}} \right), \tag{S7}$$

and

$$\alpha_- = -\ln\left(\frac{c^{\mathrm{b}}_{\mathrm{Cl}}e^{-\alpha_{\mathrm{Cl}}} + c^{\mathrm{b}}_{\mathrm{imp}}e^{-\alpha_{\mathrm{imp}}}}{c^{\mathrm{b}}_{\mathrm{Cl}} + c^{\mathrm{b}}_{\mathrm{imp}}}\right). \tag{S8}$$

S2   Calculation of the surface tension

S2.1   Derivation of the integral formula for the surface tension

First, we consider a planar system of height L with a single surface of area a. The Gibbs-Duhem relation for such a system reads

$$ad\gamma = -\sum_i N_i d\mu_i + V dp - S dT, \tag{S9}$$

where γ is the surface tension, μ_i is the chemical potential of the i-th ion, N_i is the number of the i-th ion, $V = La$ is the system volume, p is the pressure, S is the entropy, and T is the temperature.

We introduce laterally averaged concentration profiles $c_i(z)$, and we rewrite eq S9 by using $c_i(z)$. When we do not consider variation of pressure $(dp = 0)$ and temperature $(dT = 0)$, we obtain

$$d\gamma = -\sum_i \left[\int_0^L c_i(z)dz\right] d\mu_i. \tag{S10}$$

For a bulk system, the Gibbs-Duhem relation reads

$$\sum_i c^{\mathrm{b}}_i d\mu_i = dp - s^{\mathrm{b}}dT = 0, \tag{S11}$$

where $s^{\mathrm{b}} = S^{\mathrm{b}}/V$ is the bulk entropy density. Subtracting eq S11 from eq S10, we obtain

$$d\gamma = -\sum_i \left[\int_0^L (c_i(z) - c^{\mathrm{b}}_i)dz\right] d\mu_i. \tag{S12}$$

If we consider $L \to \infty$ and define the surface excess as $\Gamma_i = \int_0^\infty (c_i(z) - c^{\mathrm{b}}_i)dz$, we obtain the

Gibbs isotherm as

$$d\gamma = -\sum_i \Gamma_i d\mu_i. \tag{S13}$$

In our Poisson-Boltzmann model, the solution is considered ideal and the differential bulk chemical potential follows as $d\mu_i = (k_\mathrm{B}T/c_i^\mathrm{b})dc_i^\mathrm{b}$. By integration of eq S13, we obtain

$$\gamma = -k_\mathrm{B}T \sum_i \int_0^{c_i^\mathrm{b}} \frac{\Gamma_i}{\tilde{c}_i^\mathrm{b}} d\tilde{c}_i^\mathrm{b}. \tag{S14}$$

S2.2 Derivation of the grand potential formula for the surface tension

We derive an alternative formula for the surface tension which is needed to obtain the scaling law. This derivation follows Ref. S2. To derive the grand potential formula for the surface tension, we start with the grand potential Ω

$$\Omega(\mu, T, V, a) = -pV + \gamma a. \tag{S15}$$

From this we derive

$$\gamma = \frac{1}{a}(\Omega + pV) = \int_0^\infty (\omega(z) + p)dz, \tag{S16}$$

where $\omega(z)$ is the grand potential density. For the bulk phase, we find from the grand-canonical equation of state

$$\omega(z \to \infty) = \frac{\Omega}{V} = -p. \tag{S17}$$

Thus,

$$\gamma = \int_0^\infty \left[\omega(z) - \omega(\infty) \right] dz. \tag{S18}$$

In our mean-field model, the grand potential density is given by

$$\omega(z) = f(z) - \sum_i \mu_i c_i(z), \tag{S19}$$

where

$$f(z) = k_{\mathrm{B}}T \sum_i c_i(z) \left[\ln(c_i(z)) - 1 + U_i(z) \right] + \frac{\varepsilon \varepsilon_0}{2} (\nabla \psi)^2, \tag{S20}$$

and

$$\mu_i = \frac{df}{dc_i} = k_{\mathrm{B}}T \left[\ln(c_i(z)) + U_i(z) \right] + q_i e \psi(z). \tag{S21}$$

Therefore we obtain

$$\omega(z) = -k_{\mathrm{B}}T \sum_i c_i(z) + \frac{\varepsilon \varepsilon_0}{2} (\nabla \psi)^2 - \rho(z)\psi(z). \tag{S22}$$

We substitute eq S22 into eq S18 and integrate using the boundary conditions

$$\left. \frac{d\psi}{dz} \right|_{z=0} = 0, \quad \text{and} \quad \psi(z \to \infty) = 0, \tag{S23}$$

leading to

$$\gamma = -k_{\mathrm{B}}T \sum_i \Gamma_i - \int_0^\infty \frac{\varepsilon \varepsilon_0}{2} (\nabla \psi)^2 dz. \tag{S24}$$

S3 Derivation of asymptotic scaling laws for $\Delta\gamma$

First, we derive asymptotic scaling laws for low salinity. If the adsorption energy of the impurity ion is much larger than that of any other ionic species, $\alpha_{\mathrm{imp}} \ll -1 \ll \alpha_i|_{i \neq \mathrm{imp}}$, impurities dominate the surface charge density at $z = z^*$, denoted by σ^*, which is given by

$$\sigma^* \approx e q_{\mathrm{imp}} \Gamma_{\mathrm{imp}}, \tag{S25}$$

where $\Gamma_{\mathrm{imp}} \approx z^* c_{\mathrm{imp}}^{\mathrm{b}} e^{-q_{\mathrm{imp}}\Psi^* - \alpha_{\mathrm{imp}}}$. On the other hand, from Gouy-Chapman theory $\sigma^* = 2\sqrt{\varepsilon \varepsilon_0 k_{\mathrm{B}}T \sum_i c_i^{\mathrm{b}}} \sinh(\Psi^*/2)$[S3] where the sum includes the impurity component. If we assume $|\Psi^*| \gg 1$, then

$$\Psi^* \approx \frac{2q_{\mathrm{imp}}}{3} \ln \left[\frac{e z^* c_{\mathrm{imp}}^{\mathrm{b}} e^{-\alpha_{\mathrm{imp}}}}{\sqrt{\varepsilon \varepsilon_0 k_{\mathrm{B}}T \sum_i c_i^{\mathrm{b}}}} \right] \tag{S26}$$
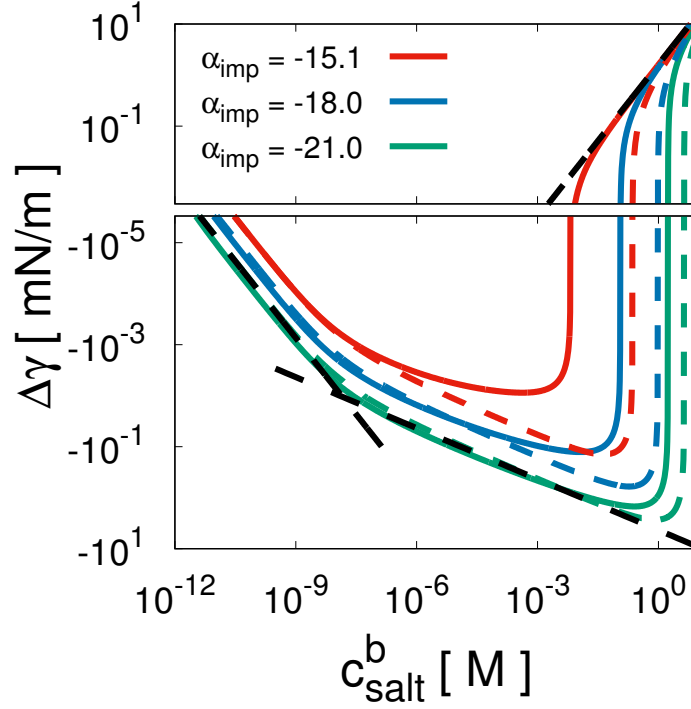
Figure S1: Surface tension $\Delta\gamma$ as a function of added electrolyte concentration, comparison between scaling laws and the full solution of the Poisson-Boltzmann model. We use $z^* = 0.5\,\mathrm{nm}$, $\alpha_{\mathrm{Na}} = 1.16$, $\alpha_{\mathrm{Cl}} = 0.98$, $\alpha_{\mathrm{cou}} = 1.07$, $c^{\mathrm{b}}_{\mathrm{imp}} = 2.8\,\mathrm{nM}$, and $q_{\mathrm{imp}} = -1$. We consider impurity surface affinities $\alpha_{\mathrm{imp}} = -15.1$ (red lines), $\alpha_{\mathrm{imp}} = -18.0$ (blue lines), and $\alpha_{\mathrm{imp}} = -21.0$ (green lines). The solid lines are full solutions of the Poisson-Boltzmann equation, whereas the colored broken lines are the heuristic scaling forms, eq S40. The black broken lines are the scaling laws for $\alpha_{\mathrm{imp}} = -21.0$, eqs S33, S34, and S38, which have slopes -1, $-1/3$, and 1 in the double-logarithmic plot, respectively.

and

$$\Gamma_{\text{imp}} \approx A \left(\frac{\sum_i c_i^{\text{b}}}{2} \right)^{1/3}, \tag{S27}$$

where

$$A = \left(\frac{2\varepsilon\varepsilon_0 k_{\text{B}} T z^* c_{\text{imp}}^{\text{b}} e^{-\alpha_{\text{imp}}}}{e^2} \right)^{1/3}. \tag{S28}$$

The charge neutrality condition, given by $\sum_i q_i \Gamma_i = 0$, shows that Γ_{imp} is compensated for by other ionic components. For example, for a negatively charged impurity and sodium as the counterion the compensation would be due to Γ_{Na}. Because the two excess adsorptions Γ_{imp} and Γ_{Na} dominate the surface tension increment in eq S24, we arrive at

$$\gamma(\{c_i^{\text{b}}\}) \approx -2Ak_{\text{B}}T \left(\frac{\sum_i c_i^{\text{b}}}{2} \right)^{1/3}. \tag{S29}$$

When we consider the four-component system (Na^+, Cl^-, impurities, and their counterion), the surface tension without added salt follows from eq S29 as

$$\gamma(c_{\text{salt}}^{\text{b}} = 0, c_{\text{imp}}^{\text{b}}) \approx -2Ak_{\text{B}}T c_{\text{imp}}^{\text{b}}{}^{1/3}. \tag{S30}$$

We define the surface tension difference due to added salt by

$$\Delta\gamma(c_{\text{salt}}^{\text{b}}) = \gamma(c_{\text{salt}}^{\text{b}}, c_{\text{imp}}^{\text{b}}) - \gamma(c_{\text{salt}}^{\text{b}} = 0, c_{\text{imp}}^{\text{b}}), \tag{S31}$$

which is zero at $c_{\text{salt}}^{\text{b}} = 0$ by definition. From eq S29, we obtain

$$\Delta\gamma(c_{\text{salt}}^{\text{b}}) = -2Ak_{\text{B}}T \left[\left(c_{\text{imp}}^{\text{b}} + c_{\text{salt}}^{\text{b}} \right)^{1/3} - c_{\text{imp}}^{\text{b}}{}^{1/3} \right]. \tag{S32}$$

For $c_{\text{salt}}^{\text{b}} \ll c_{\text{imp}}^{\text{b}}$, $\Delta\gamma$ is

$$\Delta\gamma(c_{\text{salt}}^{\text{b}}) \approx -\frac{2Ak_{\text{B}}T}{3} \frac{c_{\text{salt}}^{\text{b}}}{c_{\text{imp}}^{\text{b}}{}^{2/3}}, \tag{S33}$$

which is linear in $c_{\text{salt}}^{\text{b}}$. For $c_{\text{salt}}^{\text{b}} \gg c_{\text{imp}}^{\text{b}}$, we obtain

$$\Delta\gamma(c_{\text{salt}}^{\text{b}}) \approx \gamma(c_{\text{salt}}^{\text{b}}, c_{\text{imp}}^{\text{b}}) \approx -2Ak_{\text{B}}T c_{\text{salt}}^{\text{b}}{}^{1/3}, \tag{S34}$$

which exhibits a characteristic power law with exponent $1/3$. Note that the same exponent has been derived in the context of nanotube conductivity, based on the same mechanism.[S4]

Next, we consider the limit of high salinity. Here, a Donnan potential is created in the interfacial layer. Assuming that α_{Na} and α_{Cl} are the adsorption energies of the added salt, the potential in the interfacial layer becomes

$$\psi(z) \approx -\left(\frac{\alpha_{\text{Na}} - \alpha_{\text{Cl}}}{2}\right)\frac{k_{\text{B}}T}{e} \quad \text{for} \quad 0 < z < z^*, \tag{S35}$$

where we used the charge neutrality condition

$$c_{\text{salt}}^{\text{b}} \sum_{i=\text{Na,Cl}} q_i e^{-q_i \psi(z)/k_{\text{B}}T - \alpha_i} \approx 0 \tag{S36}$$

and we neglect the contributions due to charged impurities. Thus, the surface excesses of Na^+ and Cl^- ions are

$$\Gamma_{\text{Na}} \approx \Gamma_{\text{Cl}} \approx z^* c_{\text{salt}}^{\text{b}} \left(e^{-(\alpha_{\text{Na}} + \alpha_{\text{Cl}})/2} - 1\right). \tag{S37}$$

If we neglect the electrostatic energy contribution to the surface tension in eq S24, we obtain

$$\Delta\gamma(c_{\text{salt}}^{\text{b}}) \approx \gamma(c_{\text{salt}}^{\text{b}}, c_{\text{imp}}^{\text{b}}) \approx 2Bk_{\text{B}}T c_{\text{salt}}^{\text{b}}, \tag{S38}$$

where

$$B = z^* \left[1 - e^{-(\alpha_{\text{Na}} + \alpha_{\text{Cl}})/2}\right]. \tag{S39}$$

Adding eqs S32 and S38, we obtain a globally valid heuristic scaling form for the surface

tension due to charged impurities

$$\Delta\gamma(c_{\text{salt}}^{\text{b}}) \approx -2Ak_{\text{B}}T\left[(c_{\text{imp}}^{\text{b}} + c_{\text{salt}}^{\text{b}})^{1/3} - c_{\text{imp}}^{\text{b}}{}^{1/3}\right]$$

$$+2Bk_{\text{B}}Tc_{\text{salt}}^{\text{b}}. \tag{S40}$$

Figure S1 shows the surface tension $\Delta\gamma$ as a function of added electrolyte for the four-component system consisting of Na^+, Cl^-, impurities, and their counterion (denoted as model 1). For α_{imp} we take the exemplary values $\alpha_{\text{imp}} = -15.1$ (red lines), $\alpha_{\text{imp}} = -18.0$ (blue lines), and $\alpha_{\text{imp}} = -21.0$ (green lines). The colored solid lines are full solutions of the Poisson-Boltzmann equation, whereas the colored broken lines are the heuristic scaling form eq S40. For $\alpha_{\text{imp}} = -15.1$ (red), the agreement between the solid and broken lines is good only for very low salt concentration ($c_{\text{salt}}^{\text{b}} < 1\,\mu\text{M}$), whereas for $\alpha_{\text{imp}} = -21.0$ (green), we find overall good agreement. The three black broken lines are the scaling laws for $\alpha_{\text{imp}} = -21.0$, eqs S33, S34, and S38.

S4 Extraction of z^*, α_{Na}, and α_{Cl}

In Ref. S5, potentials of mean force for sodium and chloride ions at the air/water interface have been extracted from classical molecular dynamics simulation which employed optimized non-polarizable force fields for ions and SPC/E water. The fit expressions to the potentials of mean force were reported in the form of

$$k_{\text{B}}TU_i(z) = a_1\left[(e^{-a_2(z-a_3)} + 1)^2 - 1\right] + b_1e^{-b_2(z-b_3)^2}$$

$$-c_1(z - c_2)e^{-c_3(z-c_4)^2}, \tag{S41}$$

of which the parameter values are shown in Table S1. The potentials of mean force for sodium and chloride ions are plotted in Figure S2. We choose $z^* = 0.5\,\text{nm}$ denoted by the black broken line in Figure S2, which is close to the position where the potentials of mean
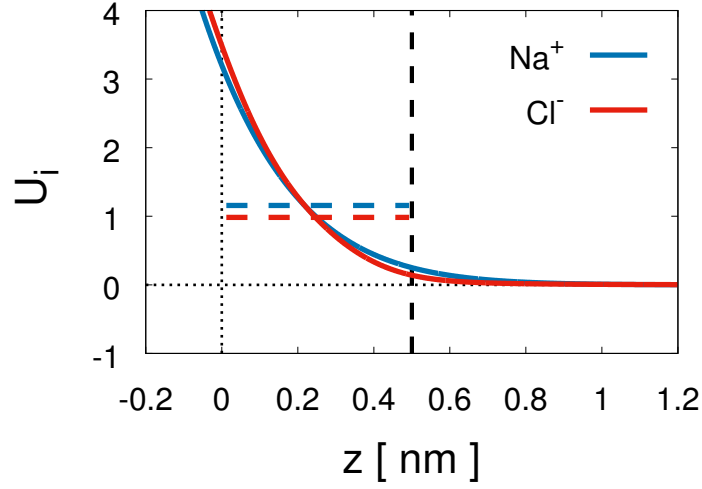
Figure S2: Potential of mean force for sodium (blue line) and chloride (red line) ions at the air/water interface from molecular dynamics simulations.[S5] The Gibbs dividing surface of water is located at $z = 0$. We choose $z^* = 0.5\,\text{nm}$ (black broken line) for the interfacial layer thickness. The colored broken lines denote $\alpha_{\text{Na}} = 1.16$ and $\alpha_{\text{Cl}} = 0.98$, respectively.

Table S1: Fit parameters for potential of mean force eq S41 from simulation data.[S5]

		Na^+	Cl^-
a_1	(kJ·mol^{-1})	0	0.0504
a_2	(nm^{-1})	-	3.891
a_3	(nm)	-	0.51978
b_1	(kJ·mol^{-1})	185.37	2.7232
b_2	(nm^{-2})	1.50	14.64
b_3	(nm)	-1.4493	0.06995
c_1	$(\text{kJ·mol}^{-1}\text{·nm}^{-1})$	0	11.227
c_2	(nm)	-	0.24253
c_3	(nm^{-2})	-	23.63
c_4	(nm)	-	-0.064528

force start to deviate from zero. We extract α_{Na} and α_{Cl} by requiring the surface excess to be identical to the simulated value in the dilute limit, which is equivalent to the equation

$$(\text{e}^{-\alpha_i} - 1)z^* = \int_{-\infty}^{0} \text{e}^{-U_i(z)}dz + \int_{0}^{\infty} (\text{e}^{-U_i(z)} - 1)dz. \tag{S42}$$

This gives the values $\alpha_{\text{Na}} = 1.16$ and $\alpha_{\text{Cl}} = 0.98$, which are denoted by colored broken lines in Figure S2.

S5 Fitting method for $\alpha_{\text{H}_3\text{O}}$, α_{OH}, α_{HCO_3}, α_{SDS} and α_{DDAC}

We use the values $\alpha_{\text{Na}} = 1.16$, $\alpha_{\text{Cl}} = 0.98$, which are the values extracted by the use of eq S42. We calculate full solutions of the Poisson-Boltzmann equation to fit the experimental data plotted in Figure 2a in the main text, and obtain $\alpha_{\text{H}_3\text{O}} = -0.9$, $\alpha_{\text{OH}} = 1.6$, $\alpha_{\text{HCO}_3} = -0.4$ up to the first decimal figure.

Similarly, we derive analytic solutions of the Poisson-Boltzmann equation for ionic surfactants (α_{SDS} or α_{DDAC}) and their respective counterion (α_{Na} or α_{Cl}). For fitting α_{SDS} and α_{DDAC} in Figure 2b in the main text, we only use the data well below the critical micelle concentrations, equal to $9\,\text{mM}$ for SDS and $16\,\text{mM}$ for DDAC.[S6] The resultant adsorption energies for the ionic surfactant are $\alpha_{\text{SDS}} = -15.6$ and $\alpha_{\text{DDAC}} = -14.5$. Such a large adsorption energy can be understood using a surface-area argument for the transfer free energy of alkanes to the water phase.[S7] We approximate a dodecane ($\text{C}_{12}\text{H}_{26}$) molecule as a cylinder with radius $r = 0.2\,\text{nm}$ (van der Waals radius of methane) and length $l = 11 \times 0.1275\,\text{nm}$ ($0.1275\,\text{nm}$ is the C-C distance of an alkane chain). Assuming the surface energy of typical alkanes to be $40\,\text{mN/m}$, and the surface area $S = 4\pi r^2 + 2\pi r l = 90\,\text{nm}^2$, we obtain the transfer energy $\Delta G \approx 21k_{\text{B}}T$, which agrees with the literature value $22k_{\text{B}}T$.[S8] These transfer energies are somewhat larger than our mean fit value $15.1k_{\text{B}}T$, which makes sense since a surfactant molecule that adsorbs to the air-water interface will not be completely surrounded by air but rather lie flat on the surface.

S6 Fitting method for c_{imp}^b

First, we fix $\alpha_{imp} = (\alpha_{SDS} + \alpha_{DDAC})/2 = -15.1$ and $\alpha_{cou} = (\alpha_{Na} + \alpha_{Cl})/2 = 1.07$. We adjust $c_{imp}^b (= c_{cou}^b)$ to fit $c_{salt}^{b,\Delta\gamma=0} = 6.5\,\mathrm{mM}$ (which is the average of the experimental data as shown in Figure S3a), where $c_{salt}^{b,\Delta\gamma=0}$ is the added electrolyte concentration at which the surface tension increment vanishes, $\Delta\gamma = 0$. When we increase c_{imp}^b, the depth of the minimum in $\Delta\gamma$ and the concentration at which the minimum occurs become larger, as shown in Figure S3a. We obtain the best fit value concentration $c_{imp}^b = 2.8\,\mathrm{nM}$. When we choose a different impurity surface affinity value $\alpha_{imp} = -9.0$ and keep $\alpha_{cou} = 1.07$, we obtain the best fit value $c_{imp}^b = 1.8\,\mu\mathrm{M}$, as shown in Figure S3b. The shape of the curves $\Delta\gamma(c_{salt}^b)$ for different c_{imp}^b is very similar between Figures S3a,b. We thus conclude that we cannot independently determine α_{imp} and c_{imp}^b by a fit to experimental data, rather, for any given value of α_{imp} we find an optimal value of c_{imp}^b that describes the experimental data equally well.

To make this more concrete, we show in Figure S4 the contour line in the plane spanned by α_{imp} and c_{imp}^b on which $c_{salt}^{b,\Delta\gamma=0} = 6.5\,\mathrm{mM}$ (black line). We also plot the contour line on which the minimum of $\Delta\gamma$ is located at a concentration of $c_{salt}^{b,min} = 1\,\mathrm{mM}$ (red line) and where the depth at the minimum is $\Delta\gamma_{min} = -0.01\,\mathrm{mN/m}$ (blue line). All these characteristic values are taken from the experimental data in Figure S3. These three lines are close to each other, meaning that our model reproduces the experimental surface tension data accurately for an entire range of fit parameters. We also show the contour line of $c_{imp}^b e^{-\alpha_{imp}} = \mathrm{const.}$ (broken line), which indicates the underlying scaling derived in Section S3.

We have checked that $\Delta\gamma(c_{salt}^b, c_{imp}^b)$ calculated by eq S14

$$\Delta\gamma(c_{salt}^b, c_{imp}^b) = -k_B T \int_0^{c_{salt}^b} \left(\frac{\Gamma_+ + \Gamma_-}{\tilde{c}_{salt}^b} \right) d\tilde{c}_{salt}^b, \tag{S43}$$

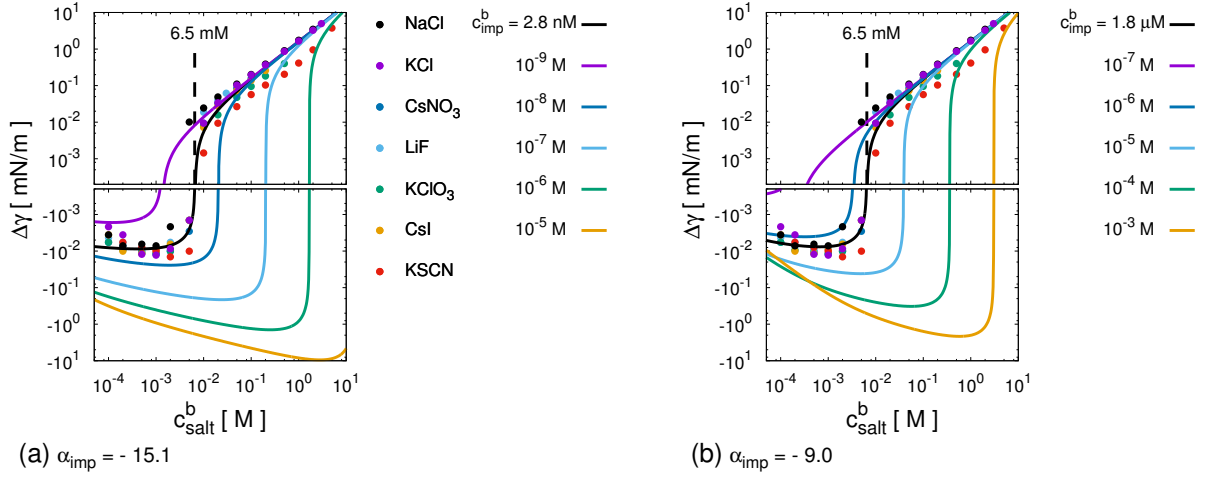is the same as $\gamma(c_{salt}^b, c_{imp}^b) - \gamma(c_{salt}^b = 0, c_{imp}^b)$ calculated by eq S24.

Figure S3: Surface tension $\Delta\gamma$ as a function of added electrolyte concentration. We use $z^* = 0.5\,\text{nm}$, $\alpha_{\text{Na}} = 1.16$, $\alpha_{\text{Cl}} = 0.98$, $\alpha_{\text{cou}} = 1.07$, $q_{\text{imp}} = -1$, and (a) $\alpha_{\text{imp}} = -15.1$ and (b) $\alpha_{\text{imp}} = -9.0$. We show curves for different values of $c_{\text{imp}}^{\text{b}}$. The black solid line shows the best fit value.
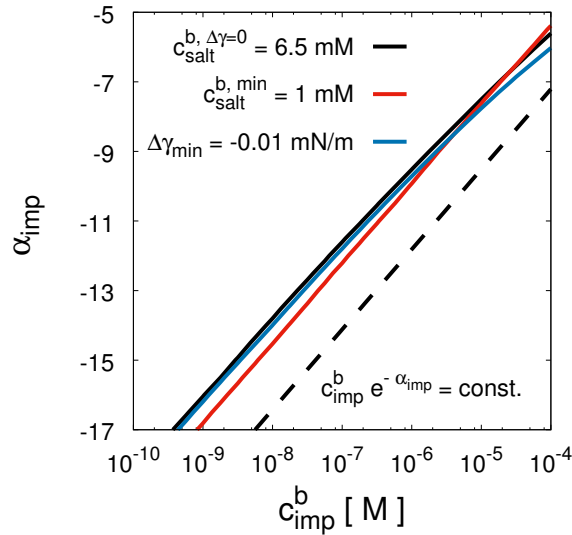

Figure S4: Contour lines of $c_{\text{salt}}^{\text{b},\Delta\gamma=0} = 6.5\,\text{mM}$, $c_{\text{salt}}^{\text{b,min}} = 1\,\text{mM}$, and $\Delta\gamma_{\text{min}} = -0.01\,\text{mN/m}$ in the plane spanned by $c_{\text{imp}}^{\text{b}}$ and α_{imp}. We use $z^* = 0.5\,\text{nm}$, $\alpha_{\text{Na}} = 1.16$, $\alpha_{\text{Cl}} = 0.98$, $\alpha_{\text{cou}} = 1.07$, and $q_{\text{imp}} = -1$.

S7   Fitting different experimental data sets

After the first measurements by Jones and Ray,[S9] the Jones-Ray effect has been reproduced in other labs.[S10–S13] While the measurements by Jones and Ray where done using the capillary rise method, different techniques have been used in later measurements, namely the twin-ring method,[S10] the bubble pressure method,[S11,S12] and the Wilhelmy plate method.[S13] The concentration of charged impurities is not precisely controlled in experiments, therefore there is no reason why the impurity concentration or the impurity type should be the same in different experiments. Here, we fit our theory to different experimental data sets.

Figure S5 shows $\Delta\gamma(c_{\mathrm{salt}}^{\mathrm{b}})$ for NaCl solutions. The capillary and bubble method data exhibit similar $c_{\mathrm{salt}}^{\mathrm{b},\Delta\gamma=0}$, thus we use the mean $c_{\mathrm{salt}}^{\mathrm{b},\Delta\gamma=0} = 3.3\,\mathrm{mM}$ to fit our theoretical curve. We use $z^* = 0.5\,\mathrm{nm}$, $\alpha_{\mathrm{Na}} = 1.16$, $\alpha_{\mathrm{Cl}} = 0.98$, $\alpha_{\mathrm{cou}} = 1.07$, $\alpha_{\mathrm{imp}} = -15.1$ and $q_{\mathrm{imp}} = -1$ and obtain $c_{\mathrm{imp}}^{\mathrm{b}} = 1.4\,\mathrm{nM}$ (black solid line), which agrees nicely with the capillary and bubble method data. The plate data consist of two measurements using H_2O and D_2O.[S13] Because the data for positive surface tension $\Delta\gamma > 0$ are not provided, we adjust $c_{\mathrm{imp}}^{\mathrm{b}}$ to fit the data points for the largest salt concentration $c_{\mathrm{salt}}^{\mathrm{b}}$. We obtain $c_{\mathrm{imp}}^{\mathrm{b}} = 25\,\mathrm{nM}$ (red solid line) for the plate method data employing H_2O and $c_{\mathrm{imp}}^{\mathrm{b}} = 48\,\mathrm{nM}$ (blue solid line) for the plate method data employing D_2O. The agreement between theory and experimental data is acceptable. The impurity concentrations for the plate method data are larger than that for the capillary and bubble method data, but still less than $100\,\mathrm{nM}$ which is the concentration of water autodissociated ions at pH $= 7$.

Figure S6 shows $\Delta\gamma(c_{\mathrm{salt}}^{\mathrm{b}})$ for KCl solutions. The capillary and bubble method data exhibit similar values of $c_{\mathrm{salt}}^{\mathrm{b},\Delta\gamma=0}$, thus we use the mean value $c_{\mathrm{salt}}^{\mathrm{b},\Delta\gamma=0} = 5.1\,\mathrm{mM}$ to fit the theory. We use $z^* = 0.5\,\mathrm{nm}$, $\alpha_{\mathrm{Na}} = 1.16$, $\alpha_{\mathrm{Cl}} = 0.98$, $\alpha_{\mathrm{cou}} = 1.07$, $\alpha_{\mathrm{imp}} = -15.1$, and $q_{\mathrm{imp}} = -1$. Because the slope of the surface tension data with respect to the salt concentration, $d\Delta\gamma/dc_{\mathrm{salt}}^{\mathrm{b}}$, of KCl solutions for high salinity is similar to that of NaCl solutions,[S14] we use the affinity $\alpha_{\mathrm{Na}} = 1.16$ also for K^+. We obtain $c_{\mathrm{imp}}^{\mathrm{b}} = 2.1\,\mathrm{nM}$ (red solid line) as a best fit for the capillary and bubble method data. The ring method data are characterized by

$c_{\text{salt}}^{\text{b},\Delta\gamma=0} = 12\,\text{mM}$, from which we obtain $c_{\text{imp}}^{\text{b}} = 5.0\,\text{nM}$ (blue solid line), which agrees quite well with the experimental data except for a few data points for low salt concentration.

The agreement between the different experimental data sets and the theoretical curves is good, provided that the impurity concentration is adjusted for each data set. Since there is no reason why different measurements should be described be the same impurity concentration or the same impurity type, this supports the idea that the Jones-Ray effect is caused by impurities.

In fact, the Jones-Ray effect disappears in the bubble pressure method when the bubble creation frequency exceeds $1/(15\,\text{sec})$.[S11] This time scale is of the order of the time it takes an impurity molecule to diffuse from the bulk to the surface, which further supports the impurity scenario.
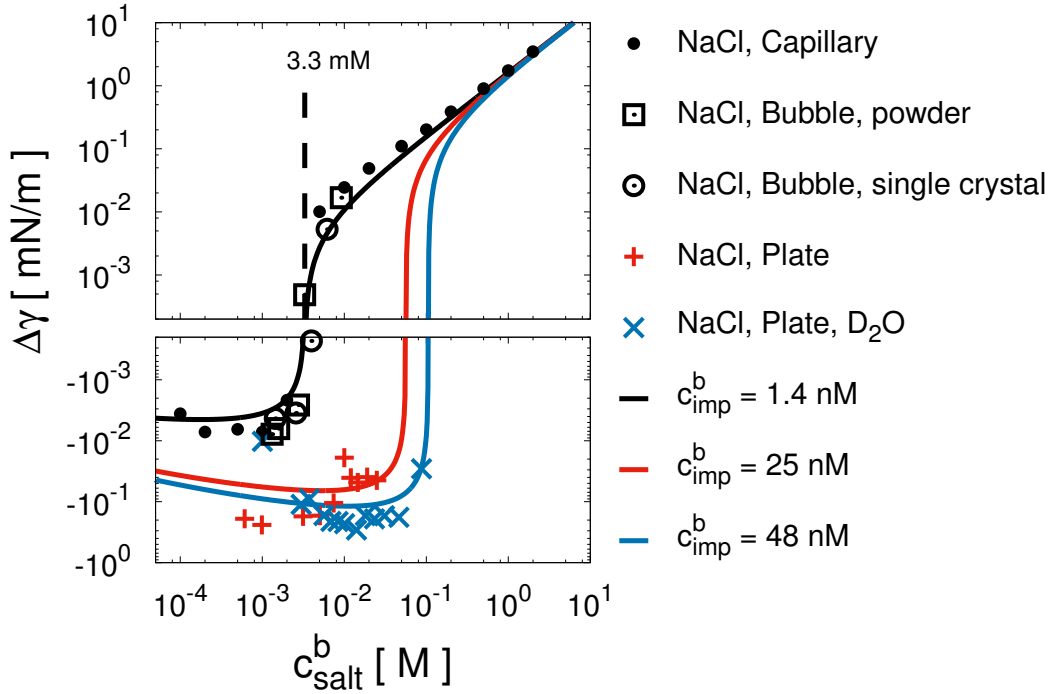

Figure S5: Comparison of different experimental data sets for the surface tension of NaCl solutions. The experimental data are obtained by the capillary rise method,[S15] the bubble pressure method,[S11] and the Wilhelmy plate method[S13] using either H_2O or D_2O as solvent. The bubble pressure method has been used with NaCl solutions from single crystals or powder. The solid lines are the theory curves obtained by adjusting $c_{\text{imp}}^{\text{b}}$. We use $z^* = 0.5\,\text{nm}$, $\alpha_{\text{Na}} = 1.16$, $\alpha_{\text{Cl}} = 0.98$, $\alpha_{\text{cou}} = 1.07$, $\alpha_{\text{imp}} = -15.1$ and $q_{\text{imp}} = -1$ in all fits.
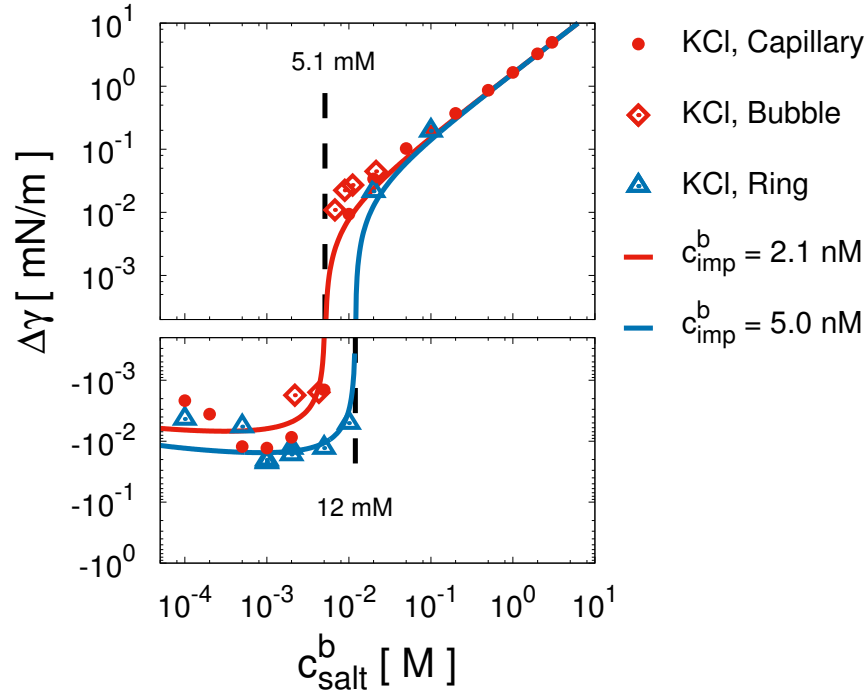
Figure S6: Comparison of different experimental data set for the KCl surface tension. The experimental data are obtained by the capillary rise method,[S16] the bubble pressure method,[S12] and the twin-ring method.[S10] The solid lines are the theory curves obtained by adjusting $c_{\mathrm{imp}}^{\mathrm{b}}$. We use $z^* = 0.5\,\mathrm{nm}$, $\alpha_{\mathrm{Na}} = 1.16$, $\alpha_{\mathrm{Cl}} = 0.98$, $\alpha_{\mathrm{cou}} = 1.07$, $\alpha_{\mathrm{imp}} = -15.1$, and $q_{\mathrm{imp}} = -1$ in all fits.

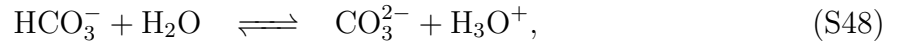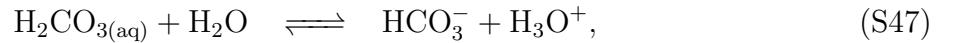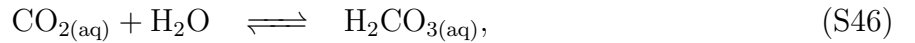# S8 Water ions and bicarbonate ions do not cause the Jones-Ray effect

Water contains hydronium and hydroxide ions due to autodissociation according to the reaction

$$2H_2O \rightleftharpoons H_3O^+ + OH^-, \tag{S44}$$

where the reaction constant is given by $K_w = c_{H_3O}^b \cdot c_{OH}^b = 10^{-14}\,M^2$. If water is in contact with ambient air, atmospheric carbon dioxide dissolves in the water according to[S17]

$$CO_{2(gas)} \rightleftharpoons CO_{2(aq)}, \tag{S45}$$

with a Henry constant $H^{cp} = c_{CO_2}^b/p_{CO_2} = 3.5 \times 10^{-2}\,M/atm,$[S17] which is equivalent to the equilibrium condition $c_{CO_2}^b/c_{CO_2}^{air} = 0.86$. The partial pressure of carbon dioxide in the atmosphere is $p_{CO_2} = 3.9 \times 10^{-4}\,atm,$[S17] which is equivalent to $c_{CO_2}^{air} = 1.6 \times 10^{-5}\,M$. In water, carbon dioxide forms carbonic acid, bicarbonate and carbonate ions according to the reactions[S17]

$$CO_{2(aq)} + H_2O \rightleftharpoons H_2CO_{3(aq)}, \tag{S46}$$

$$H_2CO_{3(aq)} + H_2O \rightleftharpoons HCO_3^- + H_3O^+, \tag{S47}$$

$$HCO_3^- + H_2O \rightleftharpoons CO_3^{2-} + H_3O^+, \tag{S48}$$

where the equilibrium constants are $K = c_{H_2CO_3}^b/c_{CO_2}^b = 2.6 \times 10^{-3}$, $K_{a1} = c_{HCO_3}^b \cdot c_{H_3O}^b/c_{H_2CO_3}^b = 1.7 \times 10^{-4}\,M$, and $K_{a2} = c_{CO_3}^b \cdot c_{H_3O}^b/c_{HCO_3}^b = 4.7 \times 10^{-11}\,M$, respectively.[S17] We neglect the reaction eq S48 because the carbonate concentration is very low. All ion concentrations are determined by chemical-equilibrium equations and the charge neutrality condition in bulk, $\sum_i q_i c_i^b = 0$. If we neglect the effect of carbon dioxide, we obtain $c_{H_3O}^b = c_{OH}^b = 10^{-7}\,M$. If we include the effect of carbon dioxide, we obtain in bulk $c_{H_3O}^b = 10^{-5.6}\,M$,

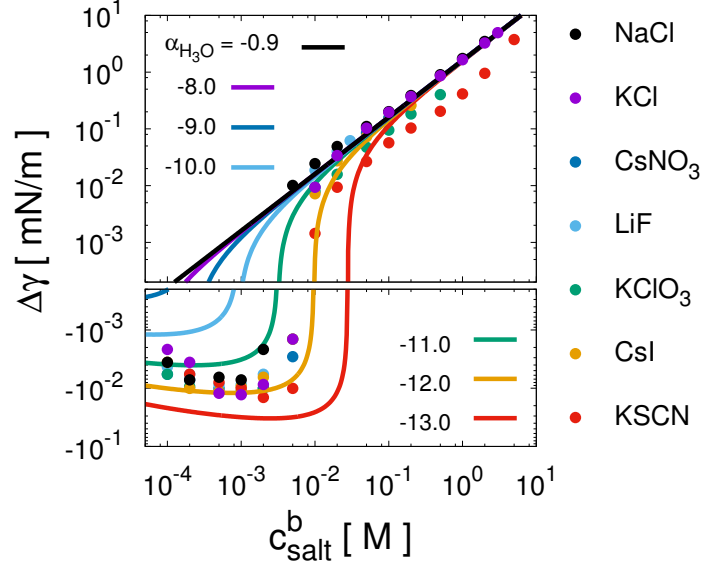$c_{OH}^b = 10^{-8.4}$ M, and $c_{HCO_3}^b \approx 10^{-5.6}$ M.

Figure S7: Effect of H_3O^+ adsorption on the surface tension of the air/water interface as a function of added electrolyte concentration. We use $z^* = 0.5$ nm, $\alpha_{Na} = 1.16$, $\alpha_{Cl} = 0.98$, $\alpha_{OH} = 1.6$, $c_{H_3O}^b = c_{OH}^b = 10^{-7}$ M, and $c_{HCO_3}^b = c_{imp}^b = c_{cou}^b = 0$. We vary α_{H_3O}. The black line is $\alpha_{H_3O} = -0.9$ extracted from the fit of the experimental HCl surface tension data.

Figure S7 shows the effect of hydronium surface adsorption on the surface tension in the absence of impurities and carbon dioxide. We use $z^* = 0.5$ nm, $\alpha_{Na} = 1.16$, $\alpha_{Cl} = 0.98$, $\alpha_{OH} = 1.6$, $c_{H_3O}^b = c_{OH}^b = 10^{-7}$ M, and $c_{HCO_3}^b = c_{imp}^b = c_{cou}^b = 0$. For $\alpha_{H_3O} = -0.9$ (black line), which follows from fitting the experimental surface tension data of HCl as shown in Figure 2a in the main text, the effect due to the surface adsorption of hydronium is almost negligible. When we set $\alpha_{H_3O} \leq -10.0$, we obtain a minimum of the surface tension which is similar to the experimental data. However, this value of $\alpha_{H_3O} \leq -10.0$ gives rise to a surface tension of HCl solutions which intensely disagrees with the experimental data, as shown by the red broken line in Figure S8.

We now include hydronium, hydroxide and carbon dioxide in the absence of impurities. For the bulk concentrations $c_{H_3O}^b = 10^{-5.6}$ M, $c_{OH}^b = 10^{-8.4}$ M, and $c_{HCO_3}^b = c_{H_3O}^b - c_{OH}^b$, we obtain the surface tension curves in Figure S9. For the realistic value $\alpha_{HCO_3} \leq -0.4$ the effect of bicarbonate surface adsorption is almost negligible. For a value of $\alpha_{HCO_3} \leq -7.0$

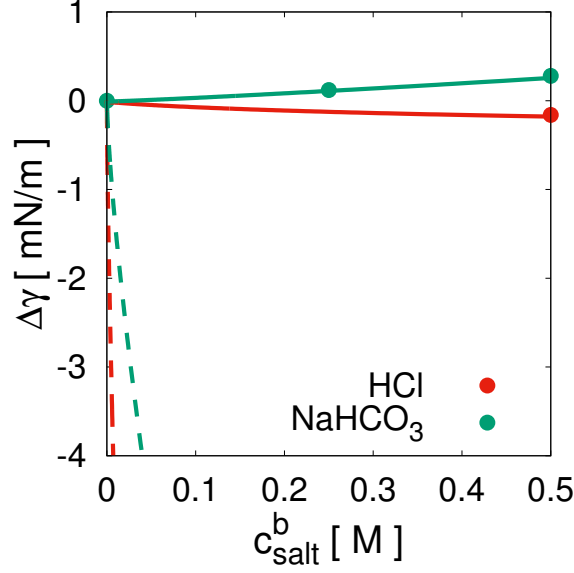Figure S8: Experimental surface tension data of HCl and $NaHCO_3$ solutions (data points). In the modeling we use $z^* = 0.5\,\text{nm}$. For HCl, we use $(\alpha_{H_3O}, \alpha_{Cl}) = (-0.9, 0.98)$ (red solid line) and $(-10.0, 0.98)$ (red broken line). For $NaHCO_3$, we use $(\alpha_{Na}, \alpha_{HCO_3}) = (1.16, -0.4)$ (green solid line) and $(1.16, -7.0)$ (green broken line). In all calculations, we do not consider impurities, water ions or carbon dioxide.
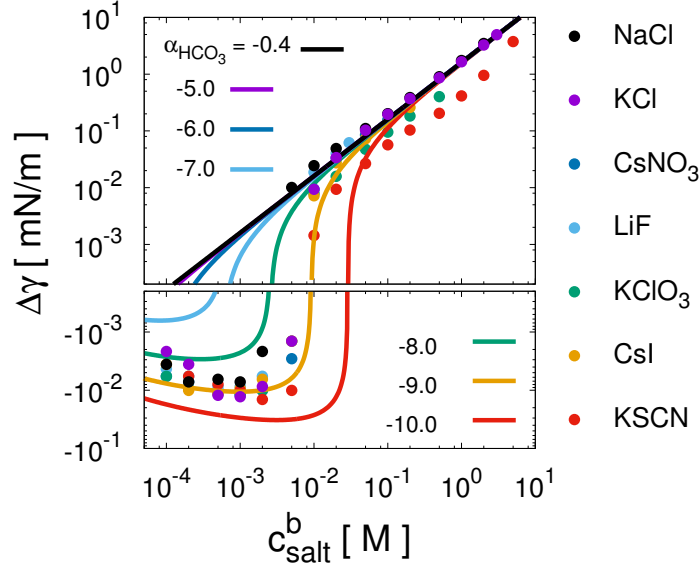
Figure S9: Effect of HCO_3^- adsorption on the surface tension of the air/water interface as a function of added electrolyte concentration. We use $z^* = 0.5\,\text{nm}$, $\alpha_{Na} = 1.16$, $\alpha_{Cl} = 0.98$, $\alpha_{H_3O} = -0.9$, $\alpha_{OH} = 1.6$, $c^b_{H_3O} = 10^{-5.6}\,\text{M}$, $c^b_{OH} = 10^{-8.4}\,\text{M}$, and $c^b_{HCO_3} \approx 10^{-5.6}\,\text{M}$, and $c^b_{imp} = c^b_{cou} = 0$. Different lines are for different values of α_{HCO_3} as indicated. The black line is for $\alpha_{HCO_3} = -0.4$ which is the value extracted from the fit to the experimental surface tension data for varying $NaHCO_3$ concentration.

we obtain a minimum in the surface tension and the experimental data is reproduced for $\alpha_{\mathrm{HCO_3}} = -9.0$. However, such strongly negative values of $\alpha_{\mathrm{HCO_3}}$ stand in intense contrast to the experimental surface tension data of $\mathrm{NaHCO_3}$ solutions, as demonstrated in Figure S8.

S9 Combined effects of impurities and water ions and bicarbonate ions

We now check whether the effect of impurities on the surface tension is significantly modified in the presence of water ions and carbon dioxide. We consider three models: in model 1 we consider added electrolyte, i.e. $\mathrm{Na^+}$ and $\mathrm{Cl^-}$ ions, charged impurities and their counterions (imp and cou); in model 2 we consider added electrolyte, charged impurities, their counterions, and in addition water ions, i.e. $\mathrm{H_3O^+}$ and $\mathrm{OH^-}$; in model 3 we consider added electrolyte, charged impurities, their counterions, water ions, and in addition bicarbonate ions, i.e. $\mathrm{HCO_3^-}$. In model 2, we assume that the bulk pH $= 7$ is independent of $c_{\mathrm{salt}}^{\mathrm{b}}$, and in model 3, we assume that the bulk pH $= 5.6$ is independent of $c_{\mathrm{salt}}^{\mathrm{b}}$.

Figure S10a shows the results for the absolute surface tension γ (not for $\Delta\gamma$) using models 1, 2, and 3. In the calculations we use $\alpha_{\mathrm{imp}} = -15.1$ and $\alpha_{\mathrm{cou}} = 1.07$, as in the main text. For extremely low $c_{\mathrm{salt}}^{\mathrm{b}}$, we observe plateaus in the surface tension curves. The red horizontal lines are the values of $\gamma(c_{\mathrm{salt}}^{\mathrm{b}} = 0, c_{\mathrm{imp}}^{\mathrm{b}})$ for model 1, 2, and 3, respectively, which follow from eq S29 with $c_{\mathrm{salt}}^{\mathrm{b}} = 0$. The red lines quantitatively agree with the plateau values predicted by models 1 and 2, but deviate slightly from the plateau value of model 3.

Figure S10b shows the impurity surface concentrations $c_{\mathrm{imp}}^{\mathrm{surf}} \equiv c_{\mathrm{imp}}(z = 0)$ (black lines) and the surface potentials (green lines) as a function of added electrolyte concentration. When we add electrolyte, the impurity surface concentration increases. However, the maximum of the surface impurity concentration does not exceed $c_{\mathrm{imp}}^{\mathrm{surf}} = 10\,\mathrm{mM}$ and thus is quite dilute.

In a slab of height L, the fraction of surface-adsorbed impurities, compared to the total
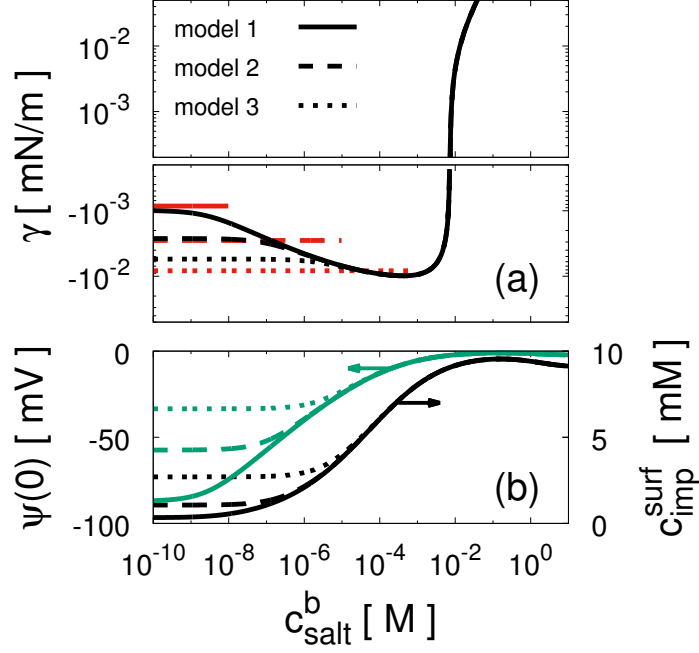
Figure S10: (a) Absolute surface tension of the air/water interface γ (not $\Delta\gamma$) as a function of added electrolyte concentration. The black solid line corresponds to results from model 1, the black broken line is for model 2, and the black dotted line is for model 3. The impurity concentration is $c_{\text{imp}}^{\text{b}} = 2.8\,\text{nM}$. We use $z^* = 0.5\,\text{nm}$, $\alpha_{\text{Na}} = 1.16$, $\alpha_{\text{Cl}} = 0.98$, $\alpha_{\text{H}_3\text{O}} = -0.9$, $\alpha_{\text{OH}} = 1.6$, $\alpha_{\text{HCO}_3} = -0.4$, $\alpha_{\text{cou}} = 1.07$, $\alpha_{\text{imp}} = -15.1$, and $q_{\text{imp}} = -1$. The red horizontal lines denote eq S29 with $c_{\text{salt}}^{\text{b}} = 0$ for model 1, 2, and 3, respectively. (b) Impurity surface concentration $c_{\text{imp}}^{\text{surf}} = c_{\text{imp}}(z = 0)$ (black lines, right axis) and surface potential (green lines, left axis) for models 1, 2, and 3 with $c_{\text{imp}}^{\text{b}} = 2.8\,\text{nM}$, respectively, as a function of electrolyte concentration.

amount of impurities, is $z^* c_{\mathrm{imp}}^{\mathrm{surf}}/L c_{\mathrm{imp}}^{\mathrm{b}}$. For a surface impurity concentration of $c_{\mathrm{imp}}^{\mathrm{surf}} = 10\,\mathrm{mM}$ and a bulk concentration of $c_{\mathrm{imp}}^{\mathrm{b}} = 2.8\,\mathrm{nM}$ we see that half of all impurities are surface-adsorbed for $L = 3\,\mathrm{mm}$. Therefore, we need a sub phase larger than $L \gg 3\,\mathrm{mm}$ in order to consider the bulk phase as a reservoir.

In Figure S10b we see that the surface potential depends sensitively on the total ionic concentration and reaches a finite value of the order of $100\,\mathrm{mV}$ for vanishing bulk electrolyte concentration.

In Figures S11a,b, we compare all three models with experimental surface tension data for the same impurity concentration $c_{\mathrm{imp}}^{\mathrm{b}} = 2.8\,\mathrm{nM}$. The differences between the three models are most pronounced at low concentrations. When we individually fit $c_{\mathrm{imp}}^{\mathrm{b}}$ to model 2 and 3, respectively, we obtain $c_{\mathrm{imp}}^{\mathrm{b}} = 3.2\,\mathrm{nM}$ for model 2 and $c_{\mathrm{imp}}^{\mathrm{b}} = 4.3\,\mathrm{nM}$ for model 3. In Figures S11c,d, we compare all three models with experimental surface tension data for the individually fitted impurity concentrations $c_{\mathrm{imp}}^{\mathrm{b}}$. The depth of the minimum does not vary, but for model 2, and more so for model 3, the comparison with experimental data is improved at low concentrations.

S10 Comparison with Onsager-Samaras theory

Onsager and Samaras considered the ionic surface excess due to the screened image interaction potential[S18]

$$U_i(z) = \frac{l_{\mathrm{B}}}{4z} \mathrm{e}^{-2\kappa z}, \tag{S49}$$

where $l_{\mathrm{B}} = e^2/4\pi\varepsilon\varepsilon_0 k_{\mathrm{B}}T$, from which they calculated the surface tension. If we include this potential into the Poisson-Boltzmann equation, the electrostatic potential vanishes, $\psi(z) = 0$, because there is no surface interaction difference between cations and anions. The resultant surface tension increment according to Onsager-Samaras theory is

$$\Delta\gamma(c_{\mathrm{salt}}^{\mathrm{b}}) = -\frac{k_{\mathrm{B}}T}{2\pi l_{\mathrm{B}}^2} \sum_{n=1}^{\infty} \frac{n^n}{n! n!} \frac{h^{n+1}}{n+1} \left(\ln h + g_n \right), \tag{S50}$$
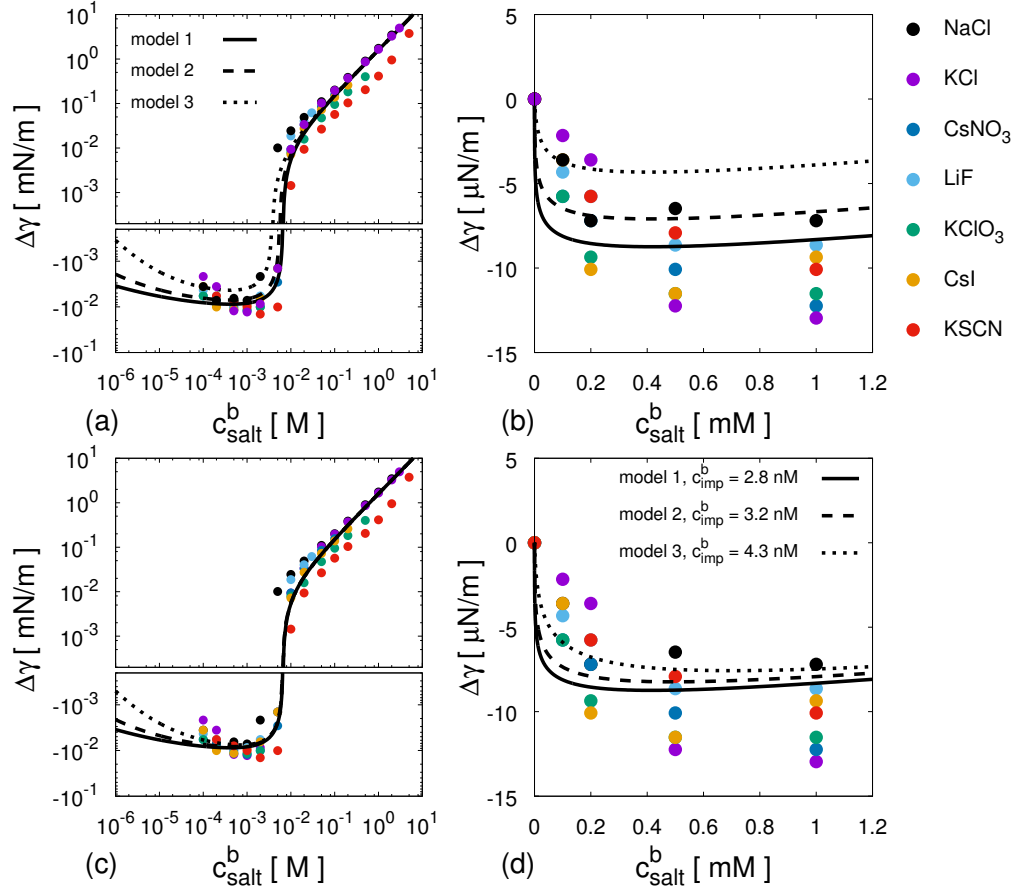
Figure S11: Comparison between the experimental data and the three different models for the surface tension of the air/water interface as a function of added electrolyte concentration. We use $z^* = 0.5\,\text{nm}$, $\alpha_{\text{Na}} = 1.16$, $\alpha_{\text{Cl}} = 0.98$, $\alpha_{\text{H}_3\text{O}} = -0.9$, $\alpha_{\text{OH}} = 1.6$, $\alpha_{\text{HCO}_3} = -0.4$, $\alpha_{\text{cou}} = 1.07$, $\alpha_{\text{imp}} = -15.1$, and $q_{\text{imp}} = -1$. The three different models are denoted by solid (model 1), broken (model 2), and dotted (model 3) lines. The impurity concentration is fixed at $c_{\text{imp}}^{\text{b}} = 2.8\,\text{nM}$ in (a) and (b), whereas it is fitted in (c) and (d). We obtain $c_{\text{imp}}^{\text{b}} = 3.2\,\text{nM}$ for model 2 and $c_{\text{imp}}^{\text{b}} = 4.3\,\text{nM}$ for model 3. (a) and (c) are double-logarithmic plots whereas (b) and (d) are linear plots.

where $h = \sqrt{2\pi l_{\mathrm{B}}^3 c_{\mathrm{salt}}^{\mathrm{b}}}$,

$$g_n = \ln n + \frac{n}{n+1} + 2C - 2\sum_{m=1}^{n} \frac{1}{m}, \tag{S51}$$

and C is Euler's constant. In the limit of $c_{\mathrm{salt}}^{\mathrm{b}} \to 0$, the derivative $d\Delta\gamma/dc_{\mathrm{salt}}^{\mathrm{b}}$ diverges.

The leading term for low concentration $(n = 1)$ is

$$
\begin{aligned}
\Delta\gamma(c_{\mathrm{salt}}^{\mathrm{b}}) &= -\frac{k_{\mathrm{B}}T}{2\pi l_{\mathrm{B}}^2} \frac{h^2}{2} (\ln h + g_1) \\
&= \mathrm{const.} \times c_{\mathrm{salt}}^{\mathrm{b}} \ln \left(\frac{\mathrm{const.}}{c_{\mathrm{salt}}^{\mathrm{b}}} \right). \tag{S52}
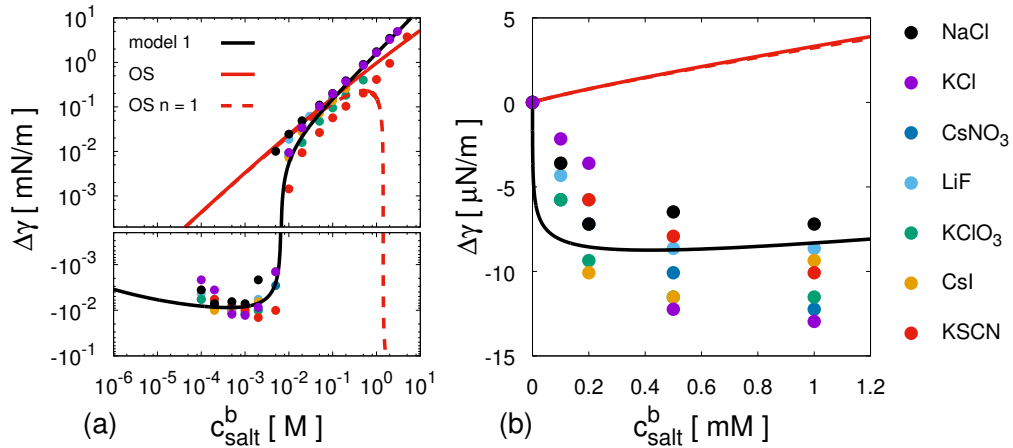\end{aligned}
$$

Figure S12: Comparison between Onsager-Samaras theory and our Poisson-Boltzmann-based model for the surface tension of the air/water interface as a function of added electrolyte concentration. We use $z^* = 0.5\,\mathrm{nm}$, $\alpha_{\mathrm{Na}} = 1.16$, $\alpha_{\mathrm{Cl}} = 0.98$, $\alpha_{\mathrm{cou}} = 1.07$, $\alpha_{\mathrm{imp}} = -15.1$, and $q_{\mathrm{imp}} = -1$. The black solid line denotes model 1 in the presence of impurities of concentration $c_{\mathrm{imp}}^{\mathrm{b}} = 2.8\,\mathrm{nM}$. The solid red line corresponds to the infinite series of OS theory, eq S50, whereas the broken red line is the leading term of OS theory, eq S52. (a) is a double-logarithmic plot whereas (b) is a linear plot.

Figure S12 shows a comparison between our Poisson-Boltzmann model, the Onsager-Samaras (OS) theory, and experiments. Note that the leading term deviates from the infinite series only for high salt concentrations $c_{\mathrm{salt}}^{\mathrm{b}} > 100\,\mathrm{mM}$. For $c_{\mathrm{salt}}^{\mathrm{b}} < 10\,\mathrm{mM}$, OS theory strongly deviates from the experimental data, since it does not capture the Jones-Ray effect. In the linear plot (b), the difference between OS theory and the experimental data comes out more clearly. Note that the diverging slope of the OS theory for very low added salt concentration

is not visible in the plots. Our theory (model 1) agrees with the experimental data over the entire concentration range.

S11   Impurities in salts

We now consider the scenario where the salt, rather than the water, contains charged surface-active impurities. We assume $q_{\mathrm{imp}} = -1$, and the impurity fraction in the added electrolyte is denoted by ν, so that the fraction of sodium and chloride ions is given by $1 - \nu$.

Figure S13 shows the calculated surface tension as a function of $c_{\mathrm{salt}}^{\mathrm{b}}$. We use $z^* = 0.5\,\mathrm{nm}$, $\alpha_{\mathrm{Na}} = 1.16$, $\alpha_{\mathrm{Cl}} = 0.98$, $\alpha_{\mathrm{cou}} = 1.07$, $q_{\mathrm{imp}} = -1$, $\alpha_{\mathrm{imp}} = -15.1$ (a), and $\alpha_{\mathrm{imp}} = -9.0$ for (b). In these calculations we do not consider additional impurities in the water, we also do not include the effects due to water ions, or bicarbonate ions.

When we require $c_{\mathrm{salt}}^{\mathrm{b},\Delta\gamma=0} = 6.5\,\mathrm{mM}$, as seen in the experimental data, we obtain $\nu = 3.8 \times 10^{-7}$ for $\alpha_{\mathrm{imp}} = -15.1$ and $\nu = 1.66 \times 10^{-4}$ for $\alpha_{\mathrm{imp}} = -9.0$. We see that the depth of minimum is significantly smaller than seen in the experiments, showing that the scenario where charged impurities are present in the added electrolyte does not explain the Jones-Ray effect.

Theoretically, the problem of finding the optimal parameters reduces to finding the apparent affinity parameters of cations and anions in eqs S7 and S8,

$$\alpha_+ = -\ln\left((1 - \nu)\mathrm{e}^{-\alpha_{\mathrm{Na}}} + \nu\mathrm{e}^{-\alpha_{\mathrm{cou}}}\right), \tag{S53}$$

and

$$\alpha_- = -\ln\left((1 - \nu)\mathrm{e}^{-\alpha_{\mathrm{Cl}}} + \nu\mathrm{e}^{-\alpha_{\mathrm{imp}}}\right). \tag{S54}$$

We analytically calculate $d\Delta\gamma/dc_{\mathrm{salt}}^{\mathrm{b}}$ in the limits of low and high salinity. In the low salinity limit, we find

$$\left.\frac{d\Delta\gamma}{dc_{\mathrm{salt}}^{\mathrm{b}}}\right|_{c_{\mathrm{salt}}^{\mathrm{b}}=0} = -k_{\mathrm{B}}Tz^*\left(\mathrm{e}^{-\alpha_+} + \mathrm{e}^{-\alpha_-} - 2\right), \tag{S55}$$

whereas in the high salinity limit, we find

$$\left.\frac{d\Delta\gamma}{dc_{\text{salt}}^{\text{b}}}\right|_{c_{\text{salt}}^{\text{b}}\to\infty} = -k_{\text{B}}Tz^* \left(2\text{e}^{-(\alpha_+ + \alpha_-)/2} - 2\right). \tag{S56}$$

From eqs S55 and S56, we determine the condition for the existence of a minimum of the function $\Delta\gamma(c_{\text{salt}}^{\text{b}})$. Figure S14 shows the region in the plane of ν and α_{imp} where the surface tension has a minimum. The red line indicates

$$\text{e}^{-\alpha_+} + \text{e}^{-\alpha_-} - 2 = 0, \tag{S57}$$

whereas the blue line indicates

$$\text{e}^{-(\alpha_+ + \alpha_-)/2} - 1 = 0, \tag{S58}$$

where α_+ and α_- are expressed by eqs S53 and S54. In region A, $d\Delta\gamma/dc_{\text{salt}}^{\text{b}} > 0$ for all $c_{\text{salt}}^{\text{b}}$, and in region C, $d\Delta\gamma/dc_{\text{salt}}^{\text{b}} < 0$ for all $c_{\text{salt}}^{\text{b}}$. Therefore, the minimum only exists in region B. We see that region B is very narrow with respect to ν, meaning that a minimum is only observed for very specific values of the impurity fraction ν.

Finally, we consider the effect of neutral impurities in the added salt, i.e. impurities for which $q_{\text{imp}} = 0$ and $c_{\text{cou}}^{\text{b}} = 0$. In our model, neutral impurities do not affect the ion distributions, and thus, the surface excess of impurities is given by

$$\Gamma_{\text{imp}} = \nu c_{\text{salt}}^{\text{b}} z^* \left(\text{e}^{-\alpha_{\text{imp}}} - 1\right). \tag{S59}$$

The ionic contribution to the surface tension is approximated by eq S38 for both low and high salinity, because the surface tension is almost linear in $c_{\text{salt}}^{\text{b}}$ for sodium chloride, as shown by the broken line in Figure 1 in the main text. The surface tension is therefore given by

$$\Delta\gamma(c_{\text{salt}}^{\text{b}}) \approx k_{\text{B}}T \left[2B(1-\nu) - \nu z^* \left(\text{e}^{-\alpha_{\text{imp}}} - 1\right)\right] c_{\text{salt}}^{\text{b}}. \tag{S60}$$
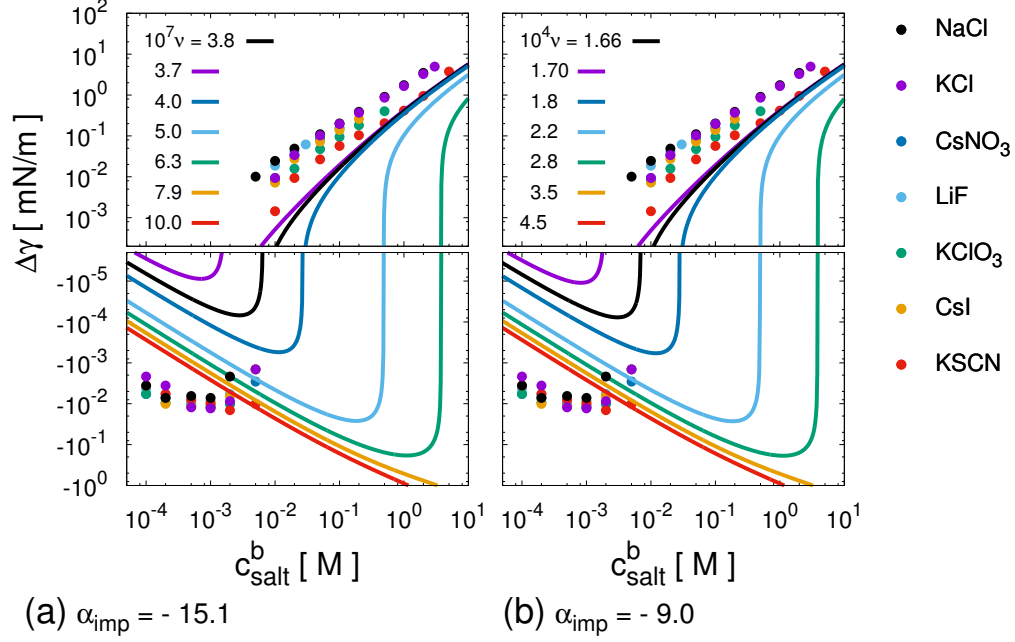
S26

Figure S13: Effect of charged impurities in added salts on the surface tension of the air/water interface. We use $z^* = 0.5\,\text{nm}$, $\alpha_{\text{Na}} = 1.16$, $\alpha_{\text{Cl}} = 0.98$, $\alpha_{\text{cou}} = 1.07$, $q_{\text{imp}} = -1$, and $c_{\text{H}_3\text{O}}^{\text{b}} = c_{\text{OH}}^{\text{b}} = c_{\text{HCO}_3}^{\text{b}} = 0$. We fix $\alpha_{\text{imp}} = -15.1$ in (a) and $\alpha_{\text{imp}} = -9.0$ in (b). We only consider impurities in the added electrolyte, not in the water. We vary the impurity fraction in the added electrolyte ν. The black solid lines are fits to $c_{\text{salt}}^{\text{b},\Delta\gamma=0} = 6.5\,\text{mM}$.
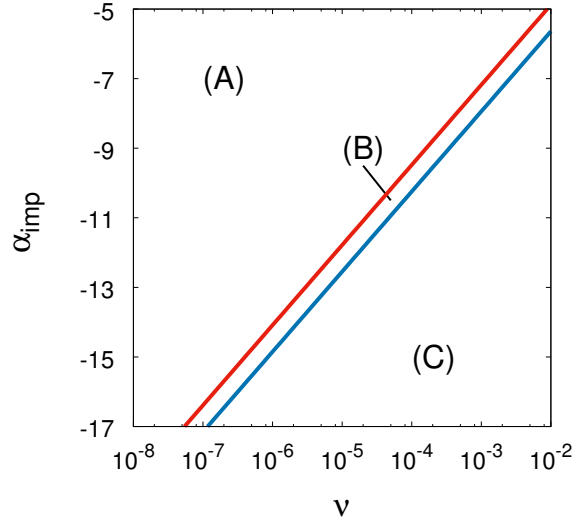

Figure S14: Phase diagram for the existence of a minimum in the surface tension in the plane of ν and α_{imp}. We use $z^* = 0.5\,\text{nm}$, $\alpha_{\text{Na}} = 1.16$, $\alpha_{\text{Cl}} = 0.98$, $\alpha_{\text{cou}} = 1.07$, $q_{\text{imp}} = -1$, and $c_{\text{H}_3\text{O}}^{\text{b}} = c_{\text{OH}}^{\text{b}} = c_{\text{HCO}_3}^{\text{b}} = 0$. We only consider impurities in the added electrolyte, not in the water. The red line is eq S57 and the blue line is eq S58. In region A, $d\Delta\gamma/dc_{\text{salt}}^{\text{b}} > 0$ for all $c_{\text{salt}}^{\text{b}}$, and in region C, $d\Delta\gamma/dc_{\text{salt}}^{\text{b}} < 0$ for all $c_{\text{salt}}^{\text{b}}$. Thus, a minimum of $\Delta\gamma(c_{\text{salt}}^{\text{b}})$ appears in region B.

Equation S60 is linear with respect to $c_{\text{salt}}^{\text{b}}$, and thus, neutral impurities in the added salt do not cause a minimum in the surface tension.

References

(S1) Abramowitz, M.; Stegun, I. A. *Handbook of Mathematical Functions*, 9th ed.; Dover Publications: New York, 1972.

(S2) Onuki, A. *J. Chem. Phys.* **2008**, *128*, 224704.

(S3) Russel, W. B.; Saville, D. A.; Schowalter, W. R. *Colloidal Dispersions*; Cambridge University Press: Cambridge, 1989.

(S4) Secchi, E.; Niguès, A.; Jubin, L.; Siria, A.; Bocquet, L. *Phys. Rev. Lett.* **2016**, *116*, 154501.

(S5) Horinek, D.; Herz, A.; Vrbka, L.; Sedlmeier, F.; Mamatkulov, S. I.; Netz, R. R. *Chem. Phys. Lett.* **2009**, *479*, 173–183.

(S6) Mukerjee, P.; Mysels, K. J. *Critical Micelle Concentration of Aqueous Surfactant Systems*; U.S. Government Printing Office: Washington, D.C., 1971.

(S7) Israelachvili, J. N. *Intermolecular and Surface Forces*, 3rd ed.; Elsevier, 2011.

(S8) Nagarajan, R.; Wang, C.-C. *Langmuir* **1995**, *11*, 4673–4677.

(S9) Jones, G.; Ray, W. A. *J. Am. Chem. Soc.* **1935**, *57*, 957–958.

(S10) Dole, M.; Swartout, J. A. *J. Am. Chem. Soc.* **1940**, *62*, 3039–3045.

(S11) Passoth, G. *Z. Physik. Chem.* **1959**, *211O*, 129–147.

(S12) Randles, J. E. B.; Schiffrin, D. J. *Trans. Faraday Soc.* **1966**, *62*, 2403–2408.

(S13) Chen, Y.; Okur, H. I.; Gomopoulos, N.; Macias-Romero, C.; Cremer, P. S.; Petersen, P. B.; Tocci, G.; Wilkins, D. M.; Liang, C.; Ceriotti, M.; Roke, S. *Sci. Adv.* **2016**, *2*, e1501891.

(S14) Pegram, L. M.; Record, M. T. *J. Phys. Chem. B* **2007**, *111*, 5411–5417.

(S15) Jones, G.; Ray, W. A. *J. Am. Chem. Soc.* **1941**, *63*, 3262–3263.

(S16) Jones, G.; Ray, W. A. *J. Am. Chem. Soc.* **1937**, *59*, 187–198.

(S17) Persat, A.; Chambers, R. D.; Santiago, J. G. *Lab on a Chip* **2009**, *9*, 2437–2453.

(S18) Onsager, L.; Samaras, N. N. T. *J. Chem. Phys.* **1934**, *2*, 528–536.